Self-Assembly of a Nonionic Photoresponsive Surfactant under Varying Irradiation Conditions: A Small-Angle Neutron Scattering and Cryo-TEM Study

Tiangang Shang, Kenneth A. Smith, and T. Alan Hatton*

Department of Chemical Engineering, Massachusetts Institute of Technology, 77 Massachusetts Avenue, Cambridge, Massachusetts 02139-4307

Received August 14, 2005. In Final Form: November 15, 2005

We have used small-angle neutron scattering (SANS), and cryogenic transmission electron microscopy (cryo-TEM) to determine the structure of aggregates formed by the photoresponsive surfactants diethylene glycol mono(4′,4-butyloxy, butyl-azobenzene) ($C_4AzoOC_4E_2$) and diethylene glycol mono(4′,4-hexyloxy, butyl-azobenzene) ($C_4AzoOC_6E_2$) under different illumination conditions. At high concentrations, the self-assembly behavior of these surfactants changes remarkably in response to different radiation conditions. The trans isomers assemble into bilamellar ($C_4AzoOC_4E_2$) and unilamellar ($C_4AzoOC_6E_2$) vesicles, while the cis isomers (under UV light) form bicontinuous phases. These light-induced structural changes are attributed to a change in the sign of the Gaussian rigidity, which is the direct result of azobenzene photoisomerization.

Introduction

Surfactants can self-assemble into micelles and other organized structures of various shapes and sizes to provide extensive applications in detergency, micellar catalysis, fabrication of mesoporous materials, micellar facilitated filtration, and many other important industrial processes.[1] A flexible and reversible method to control surfactant self-assembly is not merely of academic interest, because it can also facilitate and extend the applications of surfactants in traditional industries and in emerging high technologies. Surfactant self-assembly is determined mainly by the hydrophobic effect, for which the energy scale is on the order of several k_BT.[2] This small energy scale makes surfactant self-assembly very sensitive to variations in external conditions, in which slight changes may cause significant changes in the morphology of the self-assembled structures. This sensitivity to external conditions allows, in principle, for the active control of self-assembly. One attractive method is photocontrol using photoresponsive surfactants incorporating a group (e.g., azobenzene) that changes conformation reversibly when illumination is switched between UV and visible light. Under UV irradiation, for instance, azobenzene takes on a bent cis conformation, whereas, upon illumination with visible light, it reverts back to the planar trans conformation.[3] When the azobenzene group is incorporated into the tail of a surfactant, this reversible photoisomerization often induces changes in self-assembly behavior. Thus, self-assembly can be controlled by irradiation of different wavelengths.

Photoresponsive surfactants have been exploited in a variety of related processes, such as the regulation of metal ion permeation through vesicles,[4] the breaking and formation of vesicles,[5] photocontrolled gelation,[6] protein folding and unfolding,[7] and surface tension.[8] However, to date, no detailed study has been reported on the structural changes induced in self-assembled photoresponsive surfactant systems by changing illumination conditions. A full understanding of these light-regulated structural changes in self-assembly is not only crucial for the design and development of new photoresponsive surfactants, but can also provide new insight into the fundamentals of the self-assembly process itself.

We have synthesized an homologous series of four new, nonionic surfactants, as shown in Figure 1, in which the functional azobenzene group is located within the tail and is separated from the ethylene oxide headgroup by an alkyl spacer of *n* methylenes. These surfactants can exhibit significant differences in surface tension of about 10−12 mN/m at concentrations above the critical micelle concentration (CMC) when exposed to light of different wavelengths.[8] This large difference in surface tension strongly suggests that the structures of the aggregates in the bulk may also be very different from each other, but this issue has yet to be explored in depth.

Here, we report a detailed structural study on the self-assembly properties of two of these nonionic, azobenzene-carrying photoresponsive surfactants diethylene glycol mono(4′,4-butyloxy, butyl-azobenzene) ($C_4AzoC_4E_2$) and diethylene glycol mono(4′,4-hexyloxy, butyl-azobenzene) ($C_4AzoOC_6E_2$) as determined by small-angle neutron scattering (SANS) and cryogenic transmission electron microscopy (cryo-TEM) under both UV and visible light irradiation conditions. The results are rationalized in terms of a simple model of the effect of conformational changes on the bending and Gaussian rigidities of surfactant bilayer systems.

* Corresponding author.

(1) Hiemenz, P. C.; Rajagopalan, R. *Principles of Colloid and Surface Chemistry*, 3rd ed.; Marcel Dekker: New York, 1997

(2) Tanford, C., *The Hydrophobic Effect: Formation of Micelles and Biological Membranes*, 2nd ed.; Wiley: New York, 1979

(3) Durr, H. In *Photochromism: Molecules and Systems*; Durr, H., Bousa-Laurrent, H., Eds.; Elservier: Amsterdam, 1990; pp 1−14.

(4) Lei, Y. B.; Hurst, J. K. *Langmuir* **1999**, *15* (10), 3424−3429.

(5) Hubbard, F. P.; Santonicola, G.; Kaler, E. W.; Abbott, N. L. *Langmuir* **2005**, *21* (14), 6131−6136.

(6) Lee, C. T.; Smith, K. A.; Hatton, T. A. *Macromolecules* **2004**, *37* (14), 5397−5405.

(7) Lee, C. T.; Smith, K. A.; Hatton, T. A. *Biochemistry* **2005**, *44* (2), 524−536.

(8) Shang, T.; Smith, K. A.; Hatton, T. A. *Langmuir* **2003**, *19* (26), 10764−10773.

10.1021/la052215y CCC: $33.50
Published on Web 01/11/2006

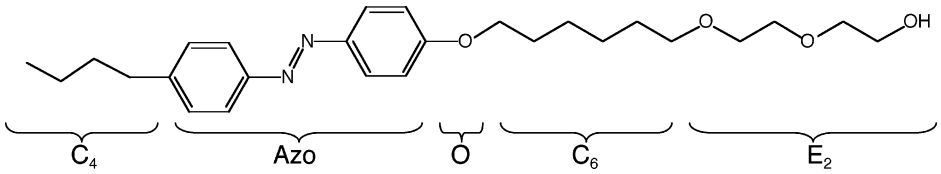

Figure 1. Molecular structure of photoresponsive surfactants $C_4AzoOC_nE_2$; the structure for $n = 6$ is shown.

Experimental Section

Synthesis. The two photoresponsive surfactants $C_4AzoOC_4E_2$ and $C_4AzoOC_6E_2$ were synthesized according to our published procedures.[8]

SANS. Neutron scattering intensities were measured as a function of scattering angle on the NG3 30 m SANS line at the National Institute of Standards and Technology (NIST) in Gaithersburg, MD. An unpolarized neutron beam with a wavelength of 6 Å (wavelength spread $\Delta\lambda/\lambda \sim 0.11$) was used in all experiments. The samples with D_2O as solvent were loaded in quartz cells with a path length of 5 mm. The scattering experiments were conducted at two sample-to-detector distances, 1.33 and 7 m, with a lateral detector offset of 0.25 m. The Q range covered in the experiment was $0.005 < Q < 0.4$ Å^{-1}. The scattering intensity on the detector was circularly averaged for each scattering angle because the sample was observed to be isotropic. Scattering from the cell itself was subtracted by assuming that it was the same as the measured scattering from an identical empty cell. The absolute scattering intensity was obtained by using NIST protocols and calibration standards. Trans samples were measured in an ambient light environment. For cis samples, the solution was first illuminated under UV light using a lamp (Oriel 6283) mounted in an arc lamp housing (Oriel 66902) powered by an arc lamp power supply (Oriel 68910) for 2 h to ensure that essentially all trans surfactants were converted to the cis form (NMR analysis in $CDCl_3$ and similar analysis of an ionic analogue at higher concentration in D_2O suggested a conversion of the trans isomer to the cis form of 92−95%). Monochromatic UV light was obtained using a 320 nm band-pass filter (Oriel 59800). Then the samples were loaded into the sample holder in the tank in which a small UV lamp was mounted to provide necessary UV illumination during experiments; this low-dose UV illumination was found to be sufficient to compensate for the slow thermal conversion of the cis isomer back to the trans form. The tank was covered by a lid to prevent the intrusion of ambient light during the measurements.

Cryo-TEM. Two different cryo-TEM techniques were utilized to visualize surfactant aggregates: replica and vitrified cryo-TEM. In all cases, trans samples were prepared under ambient light, while cis samples were first illuminated for 2 h under UV light (Oriel 6283), and the final preparation for the TEM studies was done in the dark. The time required for the preparation of the frozen sample was on the order of minutes, significantly rapid to avoid thermal isomerization of the sample back to the trans isomer, which can take hours.

The replica cryo-TEM samples were prepared through the quick freeze−deep etch (QFDE) method. First, a 1.5 μL drop of surfactant solution was deposited on the top of a metal plate, and the drop was frozen by inserting the metal plate rapidly into propane, which was cooled to about −186 °C by liquid nitrogen. Second, the frozen drop was transferred to a sealed chamber, where it was equilibrated and evaporated for 36 min under a vacuum of 10^{-7} Torr. This served to evaporate the propane and to sublime some of the water, thereby producing a bas-relief of any aggregates that were present near the drop surface. In the third step, the frozen drop was coated first with a thin platinum film of thickness 2−3 nm; and then with a 20−30 nm carbon film. Finally, the frozen drop was removed from the chamber and kept at room temperature for a few minutes. After the remaining ice had melted, the metal plate was plunged into water and the replica film floated to the water surface. The film was then placed on the grid and readied for TEM examination. The prepared samples were examined using a Philips EM410 electron microscope.

The vitrified cryo-TEM samples were prepared in a controlled-environment vitrification system (CEVS). Thin films of samples were formed by placing a 3−5 μL drop of the liquid on a holey polymer support film that had been coated with carbon and mounted on the surface of a standard TEM grid or a bare 400 mesh copper grid. The drop was then carefully blotted with filter paper until a liquid layer of approximately 50−500 nm in thickness remained across the holes in the support film. About 3−4 s after the liquid film was formed (to allow the system to relax after any shear introduced by the blotting process), it was vitrified by rapidly plunging the holey grid through a synchronous shutter at the bottom of the chamber into liquid ethane (cooled by liquid nitrogen) at its freezing point. The vitrified specimens were mounted on a cryotransfer stage (Oxford Instruments CT3500J) and examined at 100 kV in the conventional TEM mode of an analytical electron microscope (JEOL 1200EX) equipped with a twin-blade anticontaminator. The specimen temperature was maintained below −165 °C during imaging. The cryo-TEM experiments were performed by Paul Johnson of the University of Rhode Island.

Neutron Scattering Theory

In SANS, the coherent scattering intensity can be factored into two components according to[9]

$$I(Q) = nP(Q)S(Q) \tag{1}$$

where n is the number density of particles and $Q = (4\pi/\lambda)\sin\theta$, with θ as the scattering angle. $P(Q) = |F(Q)|^2$ is the form factor with $F(Q) = \int_{\text{particle}} d^3r e^{iQr}[\rho(r) - \rho_s]$, where $\rho(r)$ is the scattering length density distribution within the particle, and ρ_s is the scattering length density of the solvent. *S(Q)* is the structure factor, $S(Q) = 1/N_p \sum_i \sum_j \langle e^{iQ(R_i - R_j)} \rangle$, where $R_i - R_j$ is the center-to-center distance between two scattering aggregates. In dilute solutions, *S(Q)* is essentially 1.

Results and Analysis

SANS. Typical SANS spectra of both trans and cis $C_4AzoOC_4E_2$ and $C_4AzoOC_6E_2$ samples are shown in Figure 2. It is evident that there are significant differences in the scattering profiles for the two isomers, with scattering intensities from the trans sample being larger than those for the cis at high Q, and lower at low Q. These significant differences in SANS intensities suggest that the self-assembly behavior may be quite different for the two isomers.

SANS intensities from the trans samples were well-described by the polydispersed vesicle model, in which the vesicle core has a well-defined distribution of sizes, and the thickness of the shell is fixed. In general, for a single core−shell structure with core radius r_c and shell thickness d, whose scattering length density

(9) Higgins, J. S.; Benoît, H. C. *Polymers and Neutron Scattering*; Oxford Series on Neutron Scattering in Condensed Matter; Clarendon Press: Oxford, 1994; Vol. 8.

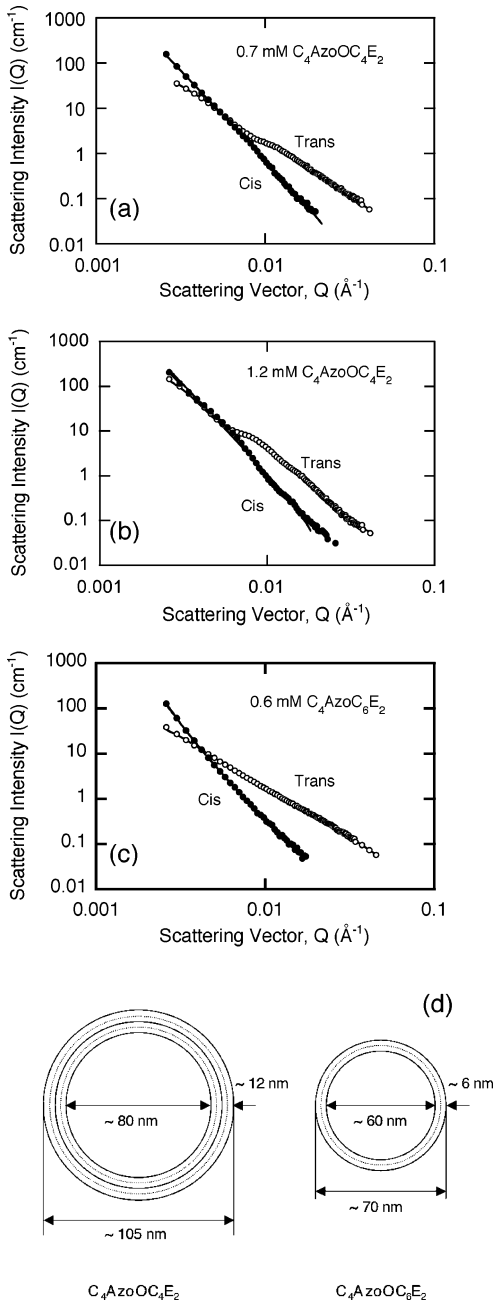

Figure 2. SANS spectra for surfactants in both trans and cis configurations. (a) 0.7 mM $C_4AzoOC_4E_2$, (b) 1.2 mM $C_4AzoOC_4E_2$, and (c) 0.6 mM $C_4AzoOC_6E_2$. (d) The relative structures of the vesicles formed for the trans samples.

(SLD) distribution can be approximated by

$$\rho(r) = \begin{cases} \rho_s & r \le r_c \\ \rho_d & r_c < r \le r_c + d \end{cases} \qquad (2)$$

the form factor is[10]

$$P(x) = |F(x)|^2 = \left|\frac{4\pi}{Q^3}(\rho_d - \rho_s)[j(x + \delta x) - j(x)]\right|^2 \qquad (3)$$

in which x is the dimensionless variable Qr_c, $\delta = d/r_c$, and $j(x) = \sin x - x \cos x$.

(10) Bartlett, P.; Ottewill, R. H. *J. Chem. Phys.* **1992**, *96* (4), 3306−3318.

Table 1. Vesicle Properties for the trans $C_4AzoOC_4E_2$ and $C_4AzoOC_6E_2$ Surfactants as Determined by SANS

	$C_4AzoOC_4E_2$		$C_4AzoOC_6E_2$
concentration (mM)	0.7	1.2	0.6
average vesicle core radius (nm)	38.4	43.5	28.1
shell thickness (nm)	11.2	12.5	5.9
polydispersity, s	0.43	0.37	0.74

The polydispersity of the core size was described by the Schultz distribution,[11] in which the normalized distribution function is defined as

$$G(r_c) = \frac{r_c^{\,z}}{\Gamma(z+1)}\left(\frac{z+1}{\bar{r}_c}\right)^{z+1} \exp\left[-\frac{r_c}{\bar{r}_c}(z+1)\right] \qquad (4)$$

where $\bar{r}_c$ is the mean core radius, and $z = (1 - s^2)/s^2$, with $s = \sigma/\bar{r}_c$ (σ^2 is the variance of the distribution). The Schultz distribution skews toward large sizes for finite z and asymptotically approaches the Gaussian distribution with increasing z; but the standard deviation diminishes as z increases, so that, in the limit $z \to \infty$, it tends to the delta function.

The form factor in the system must be averaged over the size distribution,[10] that is,

$$\bar{P}(Qr_c) = \int_0^\infty G(r_c)P(Qr_c)dr_c \qquad (5)$$

which can be integrated to yield an explicit size-averaged form factor for Schultz-distributed core−shell spheres; the final result is given in the Appendix.

The highest surfactant concentration used was on the order of 1 mM. At this concentration, the interactions between aggregates are negligible, as indicated by the fact that no correlation peak was found in the SANS spectra for either surfactant in the trans state. As a result, the structure factor was assumed to be unity for all trans samples. Thus, the theoretical scattering intensity was taken to be

$$I(Q) = n\bar{P}(Qr_c) \qquad (6)$$

where the full expression for $\bar{P}(Qr_c)$ is given explicitly as eq A-1 in the Appendix.

The SANS spectra for the trans samples were fitted by eq 6; the fits are shown together with the measured SANS spectra in Figure 2. The parameters extracted from these fits are summarized in Table 1. Since the molecular lengths of the trans forms of both $C_4AzoOC_4E_2$ and $C_4AzoOC_6E_2$ are about 2.8−2.9 nm, with the shell thicknesses being about 12 and 6 nm, respectively, we can infer that $C_4AzoOC_4E_2$ forms vesicles with shells consisting of four surfactant layers (i.e., bilamellar), whereas $C_4AzoOC_6E_2$ forms normal bilayer (i.e., unilamellar) vesicles. These vesicles are represented schematically in Figure 2d. Note that the bilamellar structure discussed here does not appear to be an artifact of the fitting procedure, as the same results were obtained for two different samples of $C_4AzoOC_4E_2$ at different concentrations (0.7 and 1.2 mM), and a unilamellar model with a bilayer thickness of about 6 nm could not be used to fit either spectrum satisfactorily. It is known that subtle differences in the balance between attractive bilayer interactions and bilayer curvature energy can lead to differences in vesicle structure, with either unilamellar or bilamellar vesicles being favored, depending on this balance.[12] The small differences between the spacer groups in the two

(11) Hayter, J. B. Structure and Dynamics of Micelles by SANS. In *Physics of Amphiphiles: Micelles, Vesicles, and Microemulsions*; Degiorgio, V., Corti, M., Eds.; North-Holland: Amsterdam, 1985.

surfactants may be sufficient to tip the balance one way or the other, hence yielding unilamellar vesicles in one case and bilamellar in the other.

In contrast, the SANS spectra for the cis isomer cannot be described by the core−shell model. Rather, these spectra were fit well by the Debye−Anderson−Brumberger (DAB) model,[13] which characterizes the scattering density function in random two-phase systems, in which two phases with different SLDs randomly interpenetrate each other and spread over the whole sample. In the DAB model, the scattering intensity, which is proportional to the density−density correlation, is given by[13]

$$I(Q) = \frac{8\pi a^3(\rho_1 - \rho_2)^2\phi_1\phi_2}{(1 + (Qa)^2)^2} \quad (7)$$

where a is the correlation length, ρ_1 and ρ_2 are the SLDs of phases 1 and 2, respectively, and ϕ_1 and ϕ_2 are the respective phase volume fractions.

All the cis samples were fit well by the DAB model, as is evident from the comparisons of the curve fits with the experimental spectra in Figure 2, which yield a correlation length, a, of about 200 nm. Once scaled by the aggregated surfactant concentrations, the curves for all three cases studied here (0.7 and 1.2 mM for $C_4AzoOC_4E_2$, and 0.6 mM for $C_4AzoOC_6E_2$) essentially collapsed onto a single curve, strongly suggesting that the structures were the same for all three samples. These results are consistent with those for some other surfactant solutions, particularly aqueous solutions of nonionic surfactants, in which bicontinuous phases show the features of a random two-phase system. In bicontinuous phases, surfactants self-assemble into a single large bilayer or multiple layers that extend over the whole system and separate the water phase into disconnected parts, each of which also extends over the sample. Such surfactant layers, which are the sole visible objects in neutron scattering, are randomly oriented and positioned in space and possess all the characteristics of a random geometry. This randomness in the surfactant layer has been captured well by the DAB model. On the basis of this analysis, we can conclude that cis photoresponsive surfactants form bicontinuous phases under the experimental conditions considered here.

Cryo-TEM. The structures inferred from the SANS analysis were confirmed by cryo-TEM images, typical examples of which are shown in Figure 3 for the trans and cis surfactant solutions. In the trans $C_4AzoOC_6E_2$ 0.6 mM sample, many spherical objects with diameters ranging from 50−70 nm were observed in the replica cryo-TEM picture (Figure 3a), indicating that this surfactant self-assembles into spherical aggregates of a size similar to that derived from the SANS analyses. Furthermore, in the vitrified cryo-TEM picture of the same system (Figure 3b), vesicle-like structures were clearly evident (the linear striations in this image have been attributed to artifacts introduced during the sample preparation). Because of the limited resolution, it is difficult to estimate the vesicle thickness from the TEM picture, but it is very likely a bilayer. These cryo-TEM images of the $C_4AzoOC_6E_2$ are both consistent with the results of the SANS analysis, which indicated that the trans $C_4AzoOC_6E_2$ surfactant self-assembles into vesicles ~70 nm in size. Similar quality cryo-TEM images were not obtained with the $C_4AzoOC_4E_2$ surfactant; the replica results indicated the formation of spherical entities, as expected, while vitrified samples yielded tantalizing images of what appeared to be bilamellar vesicles 50−100 nm in diameter, but these were not able to be confirmed definitively.

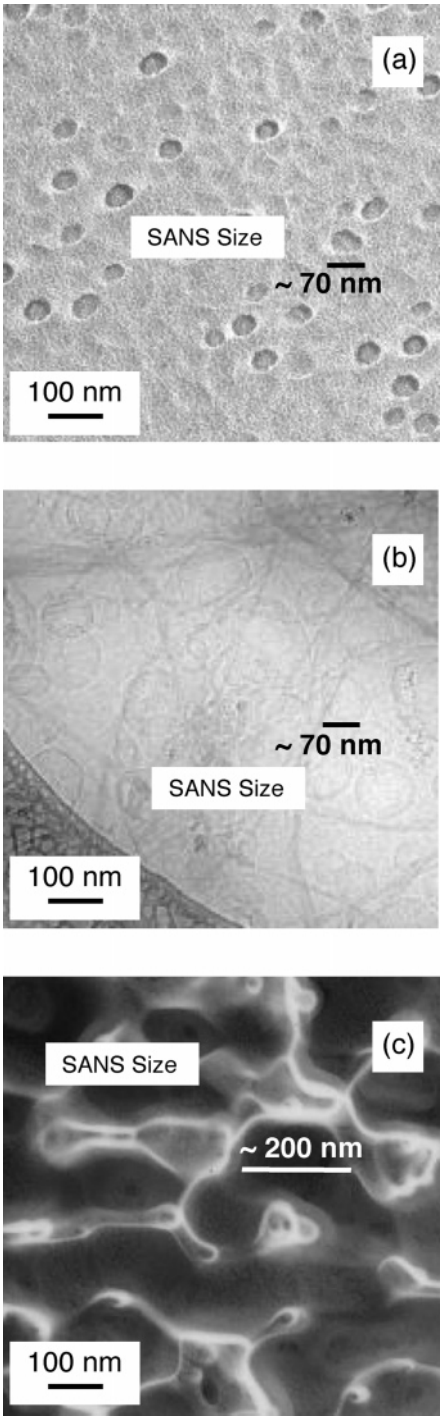

Figure 3. Cryo-TEM images of 0.6 mM $C_4AzoOC_6E_2$ photoresponsive surfactant aggregates, with scale bar showing the relevant size parameters for the structures obtained from the SANS experiments. (a) Replica image for trans conformation, which shows spherical aggregates. (b) Vitrified samples, which indicate that these aggregates are vesicles. (c) Replica image for the cis surfactant, which shows a bicontinuous structure with large aqueous domains separated by thin surfactant walls.

In the cryo-TEM picture of the cis $C_4AzoOC_6E_2$ solution (Figure 3c), there appear to be many domains of random shape and various sizes, each enclosed by a wall consisting of surfactant 5−10 nm thick, that is, about the thickness of a bilayer. This

(12) Jung, H. T.; Coldren, B.; Zasadzinski, J. A.; Iampietro, D. J.; Kaler, E. W. *Proc. Natl. Acad. Sci.* **2001**, *98* (4), 1353−1357.

(13) Roe, R. J. *Methods of X-ray and Neutron Scattering in Polymer Science*; Oxford University Press: New York, 2000.

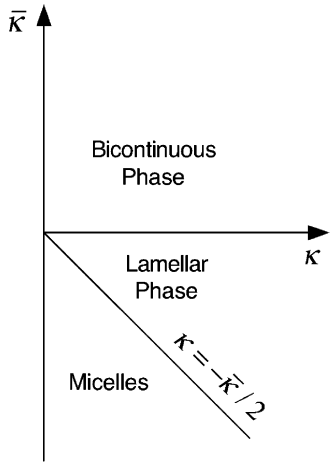

Figure 4. The phase diagram for surfactant solutions as predicted by the Helfrich elastic theory. $\bar{\kappa}$ is the Gaussian rigidity, and κ is the bending rigidity.

structure is consistent with that of a bicontinuous phase. Moreover, the average domain size was found to be around 200 nm, which is close to the correlation length extracted from the SANS spectra. No images were obtained for the cis $C_4AzoOC_4E_2$ surfactant, but its structure was expected to be similar to that of $C_4AzoOC_6E_2$, on the basis of the superpositioning of the appropriately scaled SANS spectra.

Clearly, in both cases (trans and cis $C_4AzoOC_6E_2$), the cryo-TEM results are consistent with the results from the SANS analysis and support the conclusion that the trans and cis forms of these surfactants have distinctly different aggregate morphologies. Cryo-TEM results for trans $C_4AzoOC_4E_2$ suggest that the bilamellar vesicle structures deduced from the analysis of the SANS spectra are possible, but the results are not conclusive.

Elasticity Theory and Phase Diagram

The SANS and cryo-TEM studies suggest that trans $C_4AzoOC_6E_2$ self-assembles into vesicles, whereas the cis form takes on the characteristics of a bicontinuous phase. We will attempt to offer a theoretical explanation for this interesting structural transition. First, we introduce the elastic theory of surfactant films and enunciate the various surfactant phases predicted by it. Second, a microscopic theory to calculate bending rigidity from molecular parameters is introduced to estimate the signs of the bending and Gaussian rigidities of both the trans and cis isomers from simple geometrical considerations. Finally, by combining these two theories, we can rationalize the observed structural transitions in terms of the conformational changes in the surfactants.

The behavior of surfactant membranes is captured well by a simple elastic theory, according to which the free energy density of a monolayer can be described by[14]

$$f = \frac{1}{2}\kappa_m(\sigma_1 + \sigma_2 - 2\sigma_0)^2 + \overline{\kappa_m}\sigma_1\sigma_2 \qquad (8)$$

in which κ_m and $\overline{\kappa_m}$ are the bending and Gaussian rigidities, respectively; σ_1 and σ_2 are the two principle curvatures; and σ_0, the spontaneous curvature of the monolayer, is a function of the chemical composition and molecular architecture of its constituent surfactants.

(14) Helfrich, W.; *Z. Naturforsch., C* **1973**, *28* (11-1), 693−703.

In a bilayer, both the bending and the Gaussian rigidities can be calculated from those of the monolayer:[14]

$$\kappa = 2\kappa_m$$
$$\bar{\kappa} = 2(\overline{\kappa_m} - d\sigma_0\kappa_m) \qquad (9)$$

in which d is the thickness of the bilayer. Because the chemical composition is the same in each monolayer, the bilayer spontaneous curvature is essentially zero, and thus the free energy density for the bilayer is represented by[14]

$$f = \frac{1}{2}\kappa(\sigma_1 + \sigma_2)^2 + \bar{\kappa}\sigma_1\sigma_2 \qquad (10)$$

which can be rewritten in the more convenient form,

$$f = \frac{1}{2}\left[\left(\kappa + \frac{1}{2}\bar{\kappa}\right)(\sigma_1 + \sigma_2)^2 - \frac{1}{2}\bar{\kappa}(\sigma_1 - \sigma_2)^2\right] \qquad (11)$$

From this free energy, we can construct the phase diagram of a surfactant solution in terms of κ and $\bar{\kappa}$, as shown below.

For $\kappa + \bar{\kappa}/2 > 0$ and $\bar{\kappa} < 0$, the equilibrium state is the lamellar phase in which both σ_1 and σ_2 are zero. If $\kappa + \bar{\kappa}/2 < 0$ and $\bar{\kappa} < 0$, the free energy decreases without limit as $\sigma_1 + \sigma_2$ increases, and, for any given value of either σ_1 or σ_2, will be a minimum when $\sigma_1 - \sigma_2 = 0$. This latter condition corresponds to a spherical aggregate. Above the CMC, the largest attainable curvature in spherical micellar surfactant aggregates is $1/R$, where R, the radius of the spherical micelles, is on the order of the surfactant length. Therefore, it is concluded that the spherical micellar phase is the stable phase under these conditions. Similarly, if $\kappa + \bar{\kappa}/2 > 0$ and $\bar{\kappa} > 0$, the free energy decreases without limit for $\sigma_1 - \sigma_2$ large, and, for any given value of either σ_1 or σ_2, is minimized when $\sigma_1 + \sigma_2 = 0$. This corresponds to a minimal surface, in which the average curvature $(\sigma_1 + \sigma_2)/2$ is zero everywhere. In reality, there is always some repulsive interaction originating from either steric interactions or entropy, which stabilizes the system at some finite σ. Under such circumstances, the equilibrium system is the bicontinuous phase. Finally, for $\kappa + \bar{\kappa}/2 < 0$ and $\bar{\kappa} > 0$, the bending rigidity κ is negative, which makes no sense for any real physical system. The above results are summarized in the surfactant solution phase diagram shown in Figure 4.[15] The region of this phase diagram most relevant to the self-assembly behavior of our photoresponsive surfactants is the transition from a lamellar to a bicontinuous phase, that is, where the Gaussian rigidity changes sign from negative to positive, and there is a transition from a lamellar to a bicontinuous phase. If the Gaussian rigidity of the cis isomer is positive while that of the trans is negative, then our experimental results can be explained in terms of elasticity theory. However, to apply the elasticity theory, we must estimate the sign of the Gaussian rigidity from the surfactant architecture; this is the task of the next subsection.

Petrov−Derzhanski−Mitov Model. The Petrov−Derzhanski−Mitov (PDM) model is a microscopic model relating the bending and Gaussian rigidities to the surfactant molecular parameters. According to the PDM model, the free energy per molecule in a monolayer is[16]

$$f_m = \frac{k_H}{2}\left(\frac{A_H}{H} - 1\right)^2 + \frac{k_C}{2}\left(\frac{A_C}{C} - 1\right)^2 \qquad (12)$$

(15) Kleman, M., Lavrentovich, O. D. *Soft Matter Physics: An Introduction*; Springer-Verlag: New York, 2003.

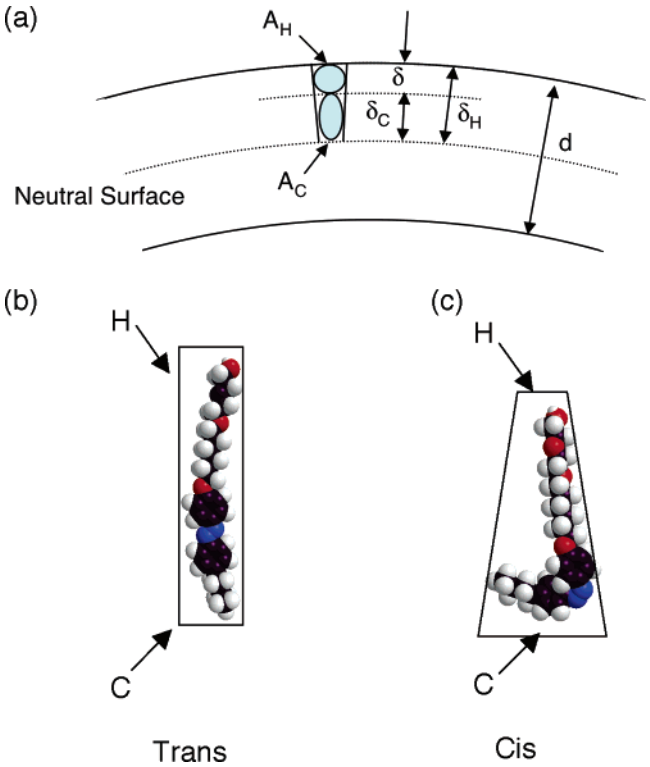

Figure 5. (a) Schematic of a bilayer defining the model parameters in the PDM model. The molecular architecture of $C_4AzoOC_6E_2$ in the (b) trans and (c) cis forms showing the difference in the head and tail-group areas for the two configurations. The equilibrium molecular architectures were computed by Gauss 94 with a 3-21 basis set.

in which k_H and k_C are the elastic constants of the interactions between heads and between tails, respectively. A_H and A_C are the cross-sectional areas actually occupied by the head and tail groups, while H and C are the corresponding cross-sectional areas in the absence of interactions. The cross-sectional areas of the head and tail groups can be calculated from[16]

$$A_H = A[1 + \delta_H(\sigma_1 + \sigma_2) + \delta_H{}^2\sigma_1\sigma_2] \qquad (13)$$

$$A_C = A[1 + \delta_C(\sigma_1 + \sigma_2) + \delta_C{}^2\sigma_1\sigma_2]$$

where A is the mean area per molecule measured at the neutral plane, in which the surfactants do not experience any strain, and δ_H and δ_C are the distances from the neutral surface to the head and tail groups, respectively, as illustrated schematically in Figure 5a.

Both the bending and the Gaussian rigidity can be obtained by substituting eq 12 into eq 13 and comparing the corresponding coefficients with those in eq 11:

$$\kappa = \left(\frac{k_H}{H^2}\delta_H{}^2 + \frac{k_C}{C^2}\delta_C{}^2\right)A_0 \qquad (14)$$

and

$$\bar{\kappa} = \frac{k_H k_C}{H^2C^2}\frac{H - C}{\dfrac{k_H}{H^2} + \dfrac{k_C}{C^2}}(\delta_C{}^2 - \delta_H{}^2) \qquad (15)$$

where $A_0 = (k_H H^{-1} + k_C C^{-1})/(k_H H^{-2} + k_C C^{-2})$ is the equilibrium area per surfactant molecule for a planar monolayer.[16]

In the symmetrical bilayer, in which the chemical components in the two monolayers are identical, the neutral surface is located exactly between the two monolayers. Under such circumstances, the distances from the neutral surface to the head and tail groups, δ_H and δ_C, respectively, can be expressed as[16]

$$\delta_H = \frac{d}{2} \text{ and } \delta_C = \frac{d}{2} - \delta \qquad (16)$$

in which d is the bilayer thickness, and $\delta = \delta_H - \delta_C$ is the distance between the head and the tail groups of the surfactant.

By substitution of eq 16 into eqs 14 and 15, the bending and Gaussian rigidities can be represented as[16]

$$\kappa = \frac{d^2}{2}\left(\frac{k_H}{H^2} + \frac{k_C}{C^2}\left(1 - \frac{2\delta}{d}\right)^2\right)\frac{\dfrac{k_H}{H} + \dfrac{k_C}{C}}{\dfrac{k_H}{H^2} + \dfrac{k_C}{C^2}} \qquad (17)$$

and

$$\bar{\kappa} = -2\delta(d - \delta)\frac{k_H k_C}{H^2C^2}\frac{H - C}{\dfrac{k_H}{H^2} + \dfrac{k_C}{C^2}} \qquad (18)$$

respectively. Therefore, the bending and Gaussian rigidities are functions of surfactant molecular architecture, which is characterized by the cross-sectional areas of the head (H) and tail (C) groups in the PDM model. The bending rigidity κ is always positive, consistent with the stability requirement for the bilayer system. However, the Gaussian rigidity $\bar{\kappa}$ can change sign with variations in the surfactant molecular architecture. Specifically, for a surfactant whose cross-sectional head area is larger than that of the tail ($H > C$), $\bar{\kappa}$ is negative. In contrast, for surfactants with a larger tail group ($H < C$), $\bar{\kappa}$ is positive. In terms of the phase diagram depicted in Figure 4, it can be concluded that, when $H > C$, surfactants self-assemble into a lamellar or, equivalently, a vesicle phase, while for $H < C$, surfactants form a bicontinuous phase.

The particular advantage of the PDM model is that we can predict the sign of the Gaussian rigidity, and therefore predict the surfactant phase behavior by using only simple geometrical arguments based on surfactant architecture. As shown in Figure 5, for the trans form, the cross-sectional area of the head, H, is similar to that of the tail, C; while, in the cis form, the headgroup area is significantly less than that of the tail group. Therefore, according to the above analysis, the trans surfactants prefer to form lamellar or vesicular phases, whereas cis surfactants self-assemble into bicontinuous phases. This conclusion is consistent with the results of the cryo-TEM and SANS studies.

Conclusions

We have investigated the self-assembly behavior of a particular pair of nonionic photoresponsive surfactants, $C_4AzoOC_4E_2$ and $C_4AzoOC_6E_2$, under different illumination conditions by SANS and, for $C_4AzoOC_6E_2$, by cryo-TEM. At high concentrations, the trans surfactants self-assemble into vesicles with either a bilayer ($C_4AzoOC_6E_2$) or a double bilayer (bilamellar; $C_4AzoOC_4E_2$) structure. In contrast, the cis surfactants form bicontinuous phases. This light-regulated structural transition

(16) Petrov, A. G. *The Lyotropic State of Matter: Molecular Physics and Living Matter Physics*; Gordon and Breach Science Publishers: Amsterdam, 1999.

originates from the change in molecular architecture accompanying trans−cis isomerization. Because of the differences in molecular architecture, the trans surfactant possesses negative Gaussian rigidity, while the cis form possesses positive Gaussian rigidity. As a consequence, trans surfactants tend to self-assemble into vesicles, while cis surfactants form a bicontinuous phase. This light-regulated structural change in self-assembly could find applications in the fabrication of microstructured objects and light-directed separation processes.

Acknowledgment. This work was supported by the Singapore-MIT Alliance and the Cambridge-MIT Institute. We wish to thank Paul Johnson of the University of Rhode Island for performing the vitrified cryo-TEM measurements.

Appendix

The form factor for polydisperse vesicles obeying the Schultz distribution obtained in closed form by the integration of eq 5 is

$$\bar{P}(x) = \frac{16\pi^2}{Q^6}(\rho_d - \rho_s)^2\left\{c_1 + c_2\bar{x} + c_3\bar{x}^2\left(\frac{z+2}{z+1}\right) + B(\bar{x})^{(z+1)/2}(c_4\cos[(z+1)D(\bar{x})] + c_7\sin[(z+1)D(\bar{x})]) + \bar{x}B(\bar{x})^{(z+2)/2}(c_5\cos[(z+2)D(\bar{x})] + c_8\sin[(z+2)D(\bar{x})]) + \left(\frac{z+2}{z+1}\right)\bar{x}^2B(\bar{x})^{(z+3)/2}(c_6\cos[(z+3)D(\bar{x})] + c_9\sin[(z+3)D(\bar{x})])\right\} \quad \text{(A-1)}$$

where the functions $B(\bar{x})$ and $D(\bar{x})$ are defined as

$$B(\bar{x}) = \frac{(z+1)^2}{(z+1)^2 + 4\bar{x}^2} \text{ and } D(\bar{x}) = \tan^{-1}\left(\frac{2\bar{x}}{z+1}\right)$$

respectively, with $\bar{x} = Q\bar{r_c}$, and the coefficients c_i are given by

$$c_1 = \frac{1}{2} - (\cos y + y\sin y) + \frac{1}{2}(1+y^2)$$

$$c_2 = y(1-\cos y)$$

$$c_3 = 1 - \cos y$$

$$c_4 = -1 - \frac{y^2}{2} + \cos y + y\sin y + (\sin y - y\cos y)^2$$

$$c_5 = -2\sin^2\left(\frac{y}{2}\right)(y + 2y\cos y - 2\sin y)$$

$$c_6 = \cos y(\cos y - 1)$$

$$c_7 = -\sin y - y\cos(2y) + \cos y(y + \sin y - y^2\sin y)$$

$$c_8 = -1 - \cos 2y + y\sin y + \cos y(2 - 2y\sin y)$$

$$c_9 = \sin y(1 - \cos y)$$

in which $y = Qd$.

LA052215Y